

UNCATALYZED AND WALL-CATALYZED FORWARD WATER-GAS SHIFT REACTION KINETICS

F. Bustamante, R. M. Enick*

National Energy Technology Laboratory - Research Associates
Department of Chemical and Petroleum Engineering
University of Pittsburgh
1249 Benedum Hall, Pittsburgh, PA, 15261

R. P. Killmeyer, B. H. Howard, K. S. Rothenberger, A. V. Cugini

U.S. Department of Energy
National Energy Technology Laboratory
P.O. Box 10940, Pittsburgh, PA 15236-0940

B. D. Morreale, M. V. Ciocco

National Energy Technology Laboratory - Support Contractors
Parsons Project Services Incorporated
Library, PA 15129

Topical Heading: Reactors, kinetics, and catalysis.

Keywords: Water-Gas Shift, kinetics, homogeneous, high-temperature, Inconel, palladium, palladium-copper alloys.

* Corresponding author: robert.enick@netl.doe.gov

UNCATALYZED AND WALL-CATALYZED FORWARD WATER-GAS SHIFT REACTION KINETICS

ABSTRACT

The kinetics of the high-temperature (1070-1134 K), low and high-pressure gas-phase forward water-gas shift reaction were evaluated in an empty quartz reactor and a quartz reactor packed with quartz particles. The power law expression for the reaction rate was consistent with the Bradford mechanism and was invariant with respect to pressure. The experimental rate constant was lower than that published by Graven and Long, and slightly higher than estimates obtained using the reaction rate expression derived from the Bradford mechanism in conjunction with values of reaction rate constants obtained from the GRI database. Similar experiments conducted using a reactor composed of Inconel[®]600, a representative reactor shell material, exhibited greatly enhanced rates of reaction. A simple power-law rate expression was incorporated into a surface-catalyzed PFR model to correlate the results between 600 – 900 K. Palladium and palladium-copper alloy surfaces, representative of hydrogen membranes, were also shown to enhance the fWGSR rate, but not as much as the Inconel[®]600 surfaces.

INTRODUCTION

The water-gas shift reaction, WGSR, Reaction 1, is well-known and used in industry as a means to increase the hydrogen yield in the production of hydrogen and/or to adjust the CO/H₂ ratio for syngas applications.



The WGSR is an equilibrium-limited reaction, with decreasing temperature favoring increased equilibrium conversion of carbon monoxide and steam to carbon dioxide and hydrogen. Therefore, the current industrial approach for the WGSR requires cooling the gasifier effluent stream before it enters the “high-temperature” water-gas shift reactor at 593-723 K. This reactor typically utilizes a packed bed of iron-chromium catalyst. The effluent from this reactor is usually fed to a “low-temperature” shift reactor at 473-523 K, which employs a copper-zinc catalyst.

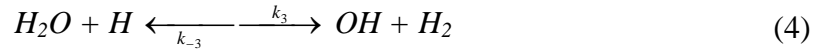
An alternative gasification plant concept studied by the U.S. Department of Energy for the production of hydrogen in the so-called Hydrogen Economy suggests carrying out the WGSR at high-temperature in a hydrogen-selective membrane reactor¹. The gasifier effluent would be filtered to remove particulates and then introduced directly

to the membrane reactor where the reaction and separation processes could be accomplished simultaneously. Unlike a conventional reactor, high conversions could be achieved at high temperature (despite the low value of the equilibrium constant) in a membrane reactor because the hydrogen partial pressure in the retentate would diminish as H_2 diffused through the membrane into the permeate stream. The permeance of most highly-selective dense membranes increases with temperature, therefore elevated temperature would result in an increased hydrogen flux. In addition, the reaction rate of the homogeneous WGSR at high temperature could be high enough that permeation through the membrane would limit reactor performance, thereby eliminating the need for the introduction of heterogeneous catalyst particles. Further, the membrane reactor would produce two streams: a high-temperature, high-pressure retentate stream containing CO_2 and steam that could be sequestered after recovering heat and condensing water from the stream, and a high-temperature, low-pressure, high-purity H_2 permeate stream that would serve as an energy source ².

The WGSR is reversible and the reaction rate of the reverse water-gas shift reaction, rWGSR, has been recently studied at elevated temperature and pressure in quartz and Inconel[®]600 reactors ³. Graven and Long ⁴ had previously conducted the only detailed study of both low-pressure, high-temperature forward and reverse WGSR. Their rWGSR rate constant values were somewhat larger than those reported in two later studies ^{5, 6}. Moreover, the difference in the energies of activation was much larger than the experimental error. Our recent paper on the rWGSR ³ addressed the discrepancies in the previous literature and showed that they could be related to the influence on the overall kinetics of the induction period where the concentration of the chain-carrier increases with time. This paper ³ also established that although a more comprehensive network of elementary steps ⁷ could be used to describe the reaction, such a network yields results nearly identical to the Bradford mechanism. However, no other complete studies on the low-pressure, high-temperature fWGSR are available in the open literature to determine whether the results published by Graven and Long ⁴ on the rate constant for the fWGSR might also be biased.

The forward reaction, fWGSR, is of more relevance to the design of post-gasifier membrane reactors than the reverse reaction, however, because the feed mixture is rich in carbon monoxide and steam. The heterogeneous fWGSR has been studied extensively ⁸⁻¹⁵ at temperatures below 873 K. Studies of the homogeneous fWGSR at elevated temperatures, $T > 1073K$, are uncommon due to the low equilibrium conversions attained in conventional reactors at those conditions. Some early investigations were performed, however, to explore the effect of the fWGSR on the oxidation of CO in the presence of water vapor ¹⁶⁻¹⁸

Mechanism of the gas-phase fWGSR Bradford ¹⁷ proposed a simple gas-phase mechanism for the WGSR. The mechanism, shown below for the fWGSR, is a chain reaction mechanism. Reaction 2 provides the chain initiation by the reaction of H_2O with any gas-phase molecule (designated by M). Reactions 3 and 4 are the propagation steps, while Reaction 5 is the termination step.



The steady-state approximation for the concentration of the chain-carriers (H and OH) leads to the following expression for the rate of reaction, Equation 6, under the conditions of low conversions:

$$r = \frac{d[CO_2]}{dt} = \left[\frac{k_1}{k_{-1}} k_2 k_3 \right]^{0.5} [CO]^{0.5} [H_2O] \quad (6)$$

The rate constant for the fWGSR is then (Equation 7),

$$k = \left[\frac{k_1}{k_{-1}} k_2 k_3 \right]^{0.5} \quad (7)$$

And the rate can be expressed as,

$$r = \frac{d[CO_2]}{dt} = k[CO]^{0.5} [H_2O] \quad (8)$$

An estimation of the energy of activation and pre-exponential factor, made by using in Equation 7 the values of k_1 , k_{-1} , k_2 , and k_3 reported in the GRI database¹⁹, gives 304.6 kJ/mol and $7.68E13 \text{ (cm}^3/\text{mol)}^{0.5} \text{ s}^{-1}$, respectively. Experimental results from Graven and Long⁴ are 274.1 kJ/mol and $7.97E12 \text{ (cm}^3/\text{mol)}^{0.5} \text{ s}^{-1}$, respectively, which yield rate constant values consistently greater than those obtained using the Bradford mechanism and GRI database, Figure 1. However, the value of the energy of activation appears to be in good agreement with the value obtained from the Bradford mechanism. Our estimation of the energy of activation and pre-exponential factor derived from the results reported by Hadman and coworkers¹⁶, i.e. utilizing Eq. 8, for the low-pressure, high-temperature (973-1073 K) fWGSR gives 319.2 kJ/mol and $2.22E14 \text{ (cm}^3/\text{mol)}^{0.5} \text{ s}^{-1}$, respectively. These parameters yield rate constant values slightly lower than those predicted from the Bradford mechanism and GRI database rate constants, and the energy of activation is also in good agreement with the value derived from the Bradford mechanism. Table 1 summarizes these estimates of the energy of activation and pre-exponential factor.

In view of the discrepancies of the previously reported rate constant values that could point out the importance of an induction period on the kinetics, the first objective of this investigation was to determine the low-pressure fWGSR at elevated temperatures and to assess the effect of high-pressure on the rate constant. The impact of the reactor walls on the reaction was determined by carrying out the reaction in an Inconel[®]600 reactor. Finally, the effect of potential membrane materials (Pd and Pd-Cu alloys) on the reaction was then determined.

EXPERIMENTAL

The experimental configuration has been described in detail elsewhere³. Briefly, the reactants were fed premixed to the reactor depicted in Figure 2. Computational Fluid Dynamics, CFD, modeling demonstrated that the reactor behaves like a laminar flow reactor, with small deviations from the ideal behavior, i.e. the average residence time was slightly lower than the expected from a tubular flow reactor³. Typically, the reactor length was set at 19 mm, giving a reactor surface area of 10.2 cm² and a volume of 1.8 cm³. Several experiments were conducted with cylindrical quartz packing (2 mm diameter, 3 mm long, 18cm², 0.7 cm³) added to the reactor, which increased the quartz surface area to 28.2 cm² while reducing the reactor volume to 1.1 cm³, thereby increasing the area/volume ratio by a factor of 4.5. The volume of the annular space, providing the rapid heat-up of the reactants from 873 K to the reaction temperature, was less than one-tenth of the reactor volume; no detectable reactant conversion occurred in that zone (control experiments with the quartz reactor had no detectable level of conversion at a temperature lower than 973 K.) An overall view of the experimental set-up is illustrated in

Figure 3. The reaction pressure was controlled with a stainless steel Badger Research pressure control valve (PCV) employing a control loop with a pressure indicator (PI). The reaction temperature was controlled with a resistance heater using a control loop with a coaxially mounted, dual element type-K thermocouple (TI) which was placed approximately 3 mm from the reactor. The temperature profile inside the reactor was determined in control experiments flowing pure gases. Typically, a deviation of +/- 5 K from the average temperature was observed over the volume of the reactor; kinetic results were corrected to account for this factor.

Only CO (99.999%) and H₂O (de-ionized) were fed to the reactor, i.e. no inert diluent gases were used. In the determination of the exponents of the rate expression, the partial pressure of one of the reactants was kept constant while the total pressure was varied. Water was injected into a CO stream through 0.125 mm ID tubing using an ISCO 500D syringe pump. The flow rate of CO (99.999%) was controlled with a Brooks 5850i mass flow controller. Tubing upstream and downstream the reactor was heated to about 423 K to prevent condensation of water before the GC analysis. This temperature imposed a maximum to the partial pressure of steam in the high-pressure experiments. Typically, the highest molar concentration of water under these conditions was 30%. A trap composed of copper oxide and alumina pellets was located in the CO inlet line before the reactor to eliminate the pronounced catalytic influence of O₂ on the reaction. This trap also removed any traces of nickel carbonyl or iron carbonyl that may have formed in the stainless steel CO cylinder. (Although deposits of carbon and elemental metal associated with the thermal decomposition of metal carbonyls could be formed on the inner wall of heated quartz tubing attached directly to the outlet of the stainless steel CO cylinder, no such deposit was observed after the trap was inserted.) Argon was continually bubbled through the water reservoir to prevent diffusion of air into the water stream. The concentration of O₂ was below detectable limits for all experiments.

A Gas Chromatograph (HP-5890 II) equipped with a TCD detector was used to quantify all the components of the reactor effluent. A porous polymer (HaySep® D) was used as column packing. Argon was employed as the carrier gas. The only detectable products in the quartz experiments were CO₂ and H₂. A CO₂/H₂ ratio greater than one (the ratio expected from the stoichiometry of the fWGSR, Reaction 1) was observed for most experiments in the quartz reactor. The CO₂/H₂ ratio at the reactor outlet was typically in the range of 1.1 – 1.4, but ratios as high as 1.9 were observed. Formation of carbonaceous particles after the reaction suggested that the higher CO conversion could be attributed to CO disproportionation, the Boudouard reaction, Reaction 9.



The build-up of carbon particles, which was observed to have some catalytic effect on the reaction, was minimized by flowing a 2 mole % O₂ in Ar after each experiment that was used to obtain conversion data for the fWGS reaction. The introduction of oxygen removed any carbon residue that had deposited within the reactor via the formation of CO₂. The effect of this high temperature oxygen exposure on palladium and palladium-copper morphology was also noted and will be discussed later in the paper. In the experiments carried out in the Inconel®600 reactor formation of methane, along with CO₂ and H₂, was observed and quantified.

Given the possibility that the Boudouard reaction could consume an appreciable amount of CO thereby increasing the CO₂/H₂ ratio at the exit of the reactor to values greater than could be attained if the fWGSR alone was occurring, the use of CO conversion would over-predict the rate of reaction and rate constant. Therefore (unless specified otherwise) the reaction rates were evaluated from the H₂O conversion, H₂O concentration and residence time. Once the CO and H₂O concentration exponents of the rate expression were elucidated, the rate constant was calculated using low-conversion data.

RESULTS AND DISCUSSION

Quartz reactor experiments

Low pressure experiments While studying the high-temperature, low-pressure fWGSR, it was critical to minimize the deposition of carbon inside the reactor. Figure 4 shows that if the reaction was conducted for a long period of time, a continuous increase in the rate of reaction was observed and significant deposits of carbon were found throughout the reactor subsequent to the experiment. This effect was not significant until about 10 hours had elapsed (Figure 4), after which the reaction rate increased steadily. Hadman and coworkers¹⁶ reported a similar effect, although they attributed it to the reactor surface becoming active for the reaction. Further, Long and Sykes¹⁸ reported that extracted charcoal (ash content lower than 0.04%) displayed a catalytic effect on the fWGSR. However, their results indicate that at high temperature (1100 K) the rate exponents for CO and H₂O approached those derived from the Bradford mechanism. Ingles²⁰ conducted a similar study using purified carbon (ash content, 0.15 wt %) instead

of coal, confirming the observation of Long and Sykes¹⁸ on the apparent predominance of the gas-phase mechanism at high temperature.

Carbon is most likely product of the Boudouard reaction, Reaction 9. This reaction is exothermic and consequently is favorable at the moderately high temperatures predominating before the inlet of the reactor. Visual inspection of the reactor after disassembly of the apparatus revealed that the carbon deposits coated a 5-cm long section of quartz surface of the pre-heating section of the reactor corresponding to the bottom of reactor detail shown in Figure 2a. The carbon particles found inside the high temperature reaction zone, where conditions did not favor the formation of carbon via the Boudouard reaction, were loose and the quartz surfaces were clean. This suggests that the carbon particles in the reaction zone actually formed in the pre-heating reaction zone and were carried by the gas flow into the reaction zone where they were retained. All the kinetic data used in the elucidation of the fWGSR rate expression presented hereafter were recorded during periods of less than eight hours. Then the O₂/Ar mixture was fed to the system until no further CO₂ was detected indicating that any carbon residue that had deposited was no longer present in the reactor. Before switching back to the reactant mixture (CO/H₂O), Ar was fed to the reactor for two hours to ensure a complete sweep of O₂ from the reactor. Although the inside of the reactor was clean, some residual carbon remained in the preheating section (temperature < 873 K). Control experiments did not show conversion of CO by the fWGSR at that low temperature, however.

The high-temperature, low-pressure fWGSR was conducted in a quartz reactor,

Figure 3. The apparatus was designed primarily to collect high-pressure data representative of coal gasification conditions; therefore few low-pressure experiments were conducted. The exponents of the CO and water concentrations in the rate expression were assumed to be 0.5 and 1.0, respectively, (the exponents predicted in Equation 6) during the analysis of these low pressure experimental results. Rate constants were determined as a function of temperature, Figure 5. The scattering of the low-pressure rate constant data was primarily attributable to experimental fluctuations in the volumetric flow rate of low-pressure steam through the reactor. The rate constants appear to be similar to the low-pressure results reported by Graven and Long⁴, although the scatter and relatively small conversions of the low pressure data do not allow for a reliable correlation for the rate constant to be established.

High-pressure experiments High-pressure experiments were conducted to confirm the exponent values of the rate expression. The best concentration exponents for CO and H₂O, as obtained from log-log plots of isothermal rate versus concentration data, were 0.49 and 0.97, respectively; values very close to those associated with the Bradford mechanism (0.5 and 1.0).

Having established the exponents of the CO and H₂O concentrations in the reaction rate expression, the temperature dependence of the rate constant value was determined between 1071 and 1121 K. Reactions were conducted in an empty quartz reactor and in the same reactor packed with quartz chopped strand. The results, provided

in Figure 6 and Table 1, indicate that the increased surface associated with the packed reactor did not influence the reaction rate. The activation energy of the NETL correlation is 288.3 kJ/mol; 5.4% less than the value of 304.6 kJ/mol associated with the Bradford mechanism/GRI database correlation and 5.0% greater than the value of 274.1 kcal/mol reported by Graven and Long. The pre-exponential constant for the NETL correlation is $7.40\text{E}11 \text{ (cm}^3/\text{mol)}^{0.5}\text{s}^{-1}$, and the rate constant values of the NETL high-pressure correlation, Figure 6, are intermediate to the Graven and Long correlation and the results obtained using Equation 6.

In our previous study³ on the kinetics of the high-temperature gas-phase *reverse* WGSR we reported that our experimental energy of activation, as well as the value reported by Graven and Long⁴, were significantly lower than those predicted from the Bradford mechanism. The difference was traced to the induction period where the increasing concentration of chain carriers with time would invalidate the assumptions used in the derivation of the rate constant from the gas-phase mechanism. A similar behavior, i.e. an induction period that would lead to the wrong prediction for the energy of activation, could be expected in the fWGSR. Simulation of the gas-phase Bradford mechanism for the fWGSR using a stiff numerical solver (ODE 23s from MatLAB[®], maximum step size = 1E-04) confirmed that under our experimental conditions neither H nor OH would achieve their stationary-state value, as shown in Figure 7. Moreover, if the concentration-time profiles from the simulations are used to evaluate the rate constant under conditions similar to the experiments (i.e., inlet concentrations, reaction time, reaction rate exponents), the resultant energy of activation (338.9 kJ/mol) is *larger* and the rate constant *lower* than the corresponding values predicted from the mechanism. On the contrary, if the simulation is run under the constraint of inlet concentrations of H and OH close to their stationary-state values, rate constants that are in excellent agreement with the derivation from the Bradford mechanism are predicted (see Figure 8). This would indicate that there was an *absence* of a significant induction period in our experiments, i.e. a relatively high inlet concentration of H and/or OH radicals was indeed achieved. Therefore, we attempted to ascertain how such conditions could be established under our experimental conditions of rapid heat-up of the mixed feed gases.

The simulation showed that at the temperature and residence time present in the preheating section, the formation of H and OH radicals from the gas-phase collisions of H₂O, Reaction 2, is extremely low and exerts a negligible effect on the high-temperature reaction. The interaction with the quartz walls would not give rise to a high concentration of radicals in the gas-phase because quartz acts a radical quencher under the experimental conditions studied here^{3, 21}. On the other hand, Ingles²⁰ suggested that the enhancing effect of carbon could be explained by its acting as chain initiator for the gas-phase reaction. In fact, steam is known to adsorb on the loosely bound atoms in graphitic surfaces. Some early experimental work has suggested that the dissociation of the H₂O molecule into H and OH is an intermediate step in the reaction between carbon and steam²². Recent computational chemistry simulations carried out by Zhu and coworkers also suggest the dissociation of steam as an important step in the water-gas shift reaction on carbon surfaces²³. Although desorption of H or OH from the surface

would provide a source of radicals at the inlet of the reactor reducing the induction period, the results of Zhu and coworkers indicate that this is not energetically favorable.

A more detailed characterization of the carbon that coated the quartz surfaces of the preheating section was conducted in an attempt to determine why there was not a significant induction period and why our reaction rates were slightly greater than expected from the Bradford mechanism. X-Ray Diffraction, XRD, analysis showed the carbon deposit to be somewhat graphitic. XRD also indicated the presence of iron silicate and metallic nickel in the carbon. It is usually recognized that silica is volatile in the presence of steam at high temperatures²⁴ which could lead to the formation of Fe(SiO₄). Scanning Electron Microscopy combined with Energy Dispersive Spectroscopy, SEM-EDS, analysis confirmed the presence of trace amounts of nickel dispersed throughout the carbon. However, iron was observed in the sample as well. Iron agglomerates in particles of irregular shape (approximately 30 μm in diameter), while nickel appears to be finely dispersed submicron particles. In addition, partial segregation was detected in some regions of the pre-heating section, Figure 9, where three distinct zones can be observed: a clean quartz surface, a thin iron layer on top of the quartz surface, and a layer of carbon deposit on top of the iron layer. A closer inspection of the last layer showed the presence of finely dispersed nickel particles. The SEM-EDS analysis was not able to determine whether the nickel is on or underneath the carbon surface due to instrumental limitations but the latter option seems more likely. Furthermore, no metal carbonyls were detected immediately downstream of the trap, and analysis of loosely bound carbon deposits upstream of the reaction zone (i.e., perhaps carried away by the flow), Figure 10, did not show the presence of nickel or iron. Therefore the most likely source of the nickel (and iron) deposited in the preheating section is the formation of nickel (and iron) carbonyl in the presence of the stainless steel tubing immediately preceding the preheating section under the CO-rich conditions as reported by Miksa and Brill²⁵. These carbonyls would then readily decompose in the hotter quartz tubing. Sykes and coworkers²⁶ studied the effects of the decomposition of nickel and iron carbonyls, formed in the cold end of stainless steel lines, on the surfaces of gas-cooled nuclear reactors at high pressure (4.1 MPa) and moderately-high temperature (623 – 973 K). They reported that nickel carbonyl promotes the deposition of carbon by forming nucleation centers in the form of small nickel particles. Once the centers are covered by carbon, the deposition process is stalled. Iron carbonyls, on the other hand, do not exert the same effect and the iron is present as agglomerates of small particles. This qualitatively agrees with our experimental observation. Moreover, the presence of nickel finely dispersed in carbon could explain why there appeared to be no significant induction period and why the conversions obtained in our study were slightly greater than those expected from the Bradford mechanism, as shown in Figure 6.

Effect of Inconel[®]600 surfaces on the fWGSR

The fWGSR was conducted in an Inconel[®]600 (approximate composition, 72% Ni, 17% Cr, 10% Fe; 3.4 cm³ volume, 17 cm² Inconel surface area) reactor to assess the potential impact that the walls of an industrial reactor might have on the gas-phase reaction at high-temperatures. There is a dramatic increase in the rate of reaction when the reaction takes place in an Inconel reactor, as shown in Figure 11. This trend is

similar to that observed for the rWGS³. For residence times of 0.5 – 1 s at 0.101 MPa, equilibrium conversions are attained for temperatures as low as 973 K in the Inconel[®]600 reactor. These results indicate that if the design of a membrane reactor with a metal shell incorporates reaction rates based on correlations obtained with quartz reactors, then the reaction rate would be significantly underestimated and the reactor volume overestimated. Further, this catalytic effect may mitigate or eliminate the need to introduce a packed bed of heterogeneous catalyst particles into the reactor².

In a previous paper we reported significant depletion of nickel and/or enrichment of chromium from the surface of Inconel[®]600 packing subjected to the rWGS³ environment. However, it is known that Ni-rich alloys can form self-healing passivation layers of chromium oxide by treatment in the presence of steam and non-oxidizing gases at very high temperature (1373 K)²⁷. Therefore, the apparent loss of nickel from the surface of the Inconel[®]600 rings could also be due to the formation of such a passivation layer. SEM-EDS and XRD characterization of the reactor wall was used to explore this possibility. The surface composition was contrasted with the bulk composition in different sections of the reactor. Three samples (e.g., 1 cm long rings) were cut from the Inconel[®]600 walls for this purpose. The cross section of the samples was polished for the SEM-EDS study; some samples were then pressed flat for subsequent XRD studies. The first ring was taken from the reaction zone (close to the top of the reactor, Figure 2b), the second from the preheating annular space close to the border of the heater, and the last one from the cold end of the reactor. The piece extracted from the reaction zone (i.e., the inner surface in the high-temperature section of the reactor) revealed the formation of a thin layer of chromium oxide on the surface of the material; the bulk composition corresponds to that of Inconel[®]600. On the contrary, analysis of the outer surface (not exposed to the reaction gases) by XRD showed the presence of a thinner layer composed of chromium oxide, nickel oxide, nickel-chromium oxide, and possibly nickel-chromium-iron oxide, attributable to high-temperature atmospheric oxidation. Therefore, the formation of the relatively thick (e.g., in the micron range) chromium oxide layer in the inside wall is due to the high-temperature WGS³ environment. Further, the depletion of nickel from the Inconel[®]600 packing would be also attributable to this cause. The second sample was extracted from the region where carbon deposits were more significant, i.e. the preheating section. The SEM analysis showed that the Ni/Cr ratio was lower on the surface than in the bulk of the wall. Moreover, surface damage is observed on the inner wall. Closer analysis of the surface revealed that the composition is not homogeneous. There are Ni-rich areas (e.g., Ni/Cr ratio is significantly higher than in the bulk of the material) separating Cr-rich zones. The former appear to be growing from the surface. This behavior is consistent with carbon diffusion into the Inconel[®]600 causing metal dusting on the surface. Indeed, SEM-EDS inspection of the carbonaceous deposit showed the presence of Ni as finely dispersed sub-micron particles. These results suggest that the metal dusting occurs primarily at the preheating section and not at the reaction zone. In other words, when the reactor operates at very high temperature (~1173 K) the gases will encounter a chromium oxide surface on the reaction zone and not metallic nickel. Finally, the ring from the cold end did not exhibit any difference between the Ni/Cr ratio on the surface and that of the bulk. Additionally, no evidence of surface attack was found.

In order to provide a preliminary correlation of the CO conversion data in the Inconel[®]600 reactor, a simple power law rate expression for equilibrium-limited reactions was incorporated into a PFR reactor model. The reaction rate was assumed to be first-order with respect to $([\text{CO}] - [\text{CO}]_{\text{eq}})$ and zeroth-order with respect to $[\text{H}_2\text{O}]$; assumptions commonly employed for commercial shift catalysts¹¹. An approach-to-equilibrium term was used to account for the reverse WGS reaction¹¹. The PFR model for a surface catalyzed reactor²⁸ was modified to account for the inner surfaces of the reactor geometry shown in Figure 2. The best-fit correlation, illustrated by the dashed line in Figure 11, was attained using an Arrhenius form of the rate constant expression with an activation energy and pre-exponential constant of 102.4 kJ/mol and 4.26E6 cm²/s, respectively, in the 600 – 900 K temperature range.

Formation of methane was observed throughout the temperature range with a peak at 973 K, Figure 12. At that temperature, the Boudouard reaction would produce a significant amount of carbon inside the reaction zone suggesting that the methane would be formed by reaction of carbon and hydrogen, Reaction 10. This reaction, which is thermodynamically favored at high-temperature, would be responsible for methane formation even at the temperature range where carbon formation is not favored due to the reactivity of the carbon-nickel deposits on the colder preheating section.



Effect of Palladium Surfaces on the fWGSR

To determine the effect of potential membrane materials, the quartz reactor was packed with pure palladium and a palladium-copper alloy (80 wt % Pd) in the form of small cylinders (2 mm diameter, 3 mm length); the total geometric surface area was chosen to be equal to the surface area of the Inconel[®]600 reactor (~20 cm²). Corresponding experiments with the quartz reactor packed with quartz packing of similar dimensions did not exhibit any effect of the packing on the reaction rate at the conditions studied. Figure 13 shows the conversions of the fWGSR in the Pd-packed reactor. Each set of data represents the average of CO conversions recorded. In all cases the reaction was run for several hours after steady state was attained (typically within the first hour of operation). However, the fresh packing displayed a slight trend of increasing conversion with time on stream during the initial hours of testing. The first data set shows a moderate increase in the reaction rate with respect to the gas-phase reaction when the reactor is packed with Pd. This increase is very small and could be within experimental error (e.g. small deviations in the actual temperature inside the reactor). Studies on the behavior of the WGSR over supported catalysts stress the importance of the redox behavior of the catalyst/support system¹⁴. At the temperature (1173 K) and net reducing environment (CO/H₂O ratio ~ 5) present during the reaction, no oxidation of Pd should be expected and the smooth Pd surface should behave like the quartz packing. However, a significant increase in CO conversion was observed after treating the Pd packing in 2% O₂/Ar overnight (data set 2). On the other hand, continuous testing for a large period of time (24 hr) without O₂/Ar treatment does not have the same effect on the observed conversions (data sets 3 and 4, Figure 13). Moreover, Figure 13 shows that the repeated

switching between oxidizing (O₂-rich) and reducing (CO-rich) environments enhances the reaction even further (increase in conversion from data set 2 to data set 3). This enhancing effect appears to be both directly proportional to the duration of the O₂ treatment and irreversible. Figure 14 compares the conversions observed in switching from high-pressure to low-pressure with a long (66 hr) intermediate O₂/Ar treatment of the Pd packing. Despite the decrease in pressure, which should translate into lower conversions due to the lower residence time and inlet concentrations, conversions in the low-pressure regime are significantly larger.

The complexity of the Pd – O₂ system is recognized by the many papers written on the subject^{29, 30, 31}. Pd-O₂ interactions are thought to lead to the occurrence of several oxygen-containing species - chemisorbed oxygen on the surface, surface palladium oxide, and bulk palladium oxide. Wolf and coworkers modeled the behavior of polycrystalline Pd under oxidation-reduction cycles³¹ and suggested a complex relationship between these three types of Pd-O interaction. Even though PdO is not expected to be stable at temperatures greater than 973 K, some remaining chemisorbed O could still be present at the surface³¹. If these oxygen species are responsible for the enhancement of conversion, sweeping the reactor with a reducing atmosphere should somewhat decrease the conversions and partly restore the conversions observed with the fresh Pd packing. An attempt was made to study this possibility. After the O₂/Ar treatment, the reactor was flushed with He and then H₂/He was admitted to the reactor. No significant change in conversions was observed upon feeding the CO/H₂O stream after the reducing treatment. However, PdO is thermodynamically stable at the conditions of our high-pressure testing³². This bulk PdO could decompose and release oxygen to the surface³¹. Consequently, we oxidized the Pd packing at the high partial pressure of oxygen used in the O₂/Ar treatment and cooled down under inert gas. The packing was characterized by means of XPS and SEM-EDS. XPS results of the as-received Pd-packing samples showed the presence of PdO, but after a mild Ar ion etch of the surface only Pd was observed. This result shows that very little surface oxide was present following the O₂/Ar treatment and that the oxide detected could be partially due to atmospheric contact during handling. More relevant are the results of the SEM study. Figure 15 depicts the surface of the fresh palladium pellets and the same pellets after reaction. There is a very noticeable roughening of the surface. This roughening is also observed in a cross section of a packing pellet as a pore-like structure extending about 50 μm into the Pd bulk. (

Figure 16). Similar changes in the morphology of supported³³ and unsupported³⁴ palladium films after treatment in O₂-rich environments at elevated temperatures has been reported. Monteiro and coworkers³⁴ reported an increase in the rate (one order of magnitude) of methane oxidation on Pd-foils after the sample was treated in a CH₄-O₂ environment (excess methane) at 598 K for less than 3 hr. However, the foils tended to deactivate with time on stream and recovered the original activity upon repeating the activation treatment. The deactivation was traced to the loss of PdO surface area due to the presence of the water produced in the reaction. Our results, on the contrary, suggest a continuous increase in activity without any indication of deactivation with time on stream (test were conducted for periods of 6 hr before O₂/Ar treatment). A possible explanation of the increase in activity is the observation by Matolin and coworkers³⁵ that CO interaction with Pd surfaces is enhanced by the presence of defects on the surface. We

cannot, however, provide a definite explanation at this point. The change in the morphology of palladium would pose a significant risk of failure if ultra-thin (<10 μm) Pd-membranes are to be used in a membrane reactor. Therefore, the operating conditions of such a membrane reactor should be carefully selected to minimize the formation of carbon since O_2 could not be used to remove any carbon build-up.

Effect of Palladium-Copper Surfaces on the fWGSR

The WGSR was also conducted in the presence of a PdCu alloy. Previous work conducted at NETL has shown that the 80 wt % Pd – Cu alloy displays sulfur tolerance over a wide range of temperature³⁶, as well as hydrogen permeation similar to pure palladium³⁷. Therefore, this alloy could be a potential candidate for membrane reactors in harsh environments. The PdCu-packing test was carried out under similar conditions as the Pd-packing test, e.g., surface area, packing shape, inlet concentrations. However, the test was restricted to ambient pressure in order to study the behavior of the alloy at the low residence times likely to be encountered in a practical application of a membrane reactor. Figure 17 shows the conversions in the PdCu-packed, quartz reactor. The fresh packing, i.e. without any pretreatment (data set 1), appears to be more active than its Pd counterpart. Moreover, the fresh packing displayed a slight but clear trend of increasing conversion with time on stream. Several hours were elapsed before the steady-state conversions reported on Figure 17 were attained. Similar to the observations with the Pd-packed reactor, there is a noticeable increase in the activity of the PdCu pellets after the packing was treated with oxygen (data set 2). Attempts to reverse the effect of the oxidizing environment by means of an extended reducing treatment (H_2/Ar in a dry environment for over 60 hours) did not induce any change in the activity of the packing (data set 3). Finally, continuous operation in the $\text{CO}/\text{H}_2\text{O}$ environment (data sets 4, 5, and 6) did not effect conversions. Although CO conversions obtained in the early stages of testing of the PdCu packing are larger than the conversions in the Pd-packed reactor under similar conditions of time on stream and oxidizing-reducing cycling (i.e. data sets 1 and 2 in Figure 13 and Figure 17, respectively), the difference in conversions in both reactors tend to level-off at longer times on stream.

The increase in the activity of the palladium packing was correlated to the change in surface area and/or morphology of the pellets. The PdCu packing was removed to determine whether such surface changes were evident in the PdCu pellets. During reaction condition exposure the PdCu pellets fused together forming a single unit while retaining their macroscopic shape; conversely, the Pd pellets remained loose following use. Moreover, numerous cracks were found on the surface of the PdCu pellets which developed into internal porosity (Figure 18). Clearly, this macroscopic/microscopic channel network would provide a more favorable environment for a heterogeneous reaction than the offered by the randomly packed palladium. Consequently, a direct comparison between the conversions in both systems is difficult. An attempt to prevent the formation of the macroscopic structure shown in Figure 18 was done. Small slabs (10 mm long, 2 mm wide, 1 mm thick) were cut from a PdCu alloy foil and twisted to form small spirals providing a less densely-packed arrange that would minimize the contact points while having the same exposed surface area. CO conversions larger than the gas-phase conversion (e.g. 2.79% versus 0.34%) were attained. However, mass transfer

limitations were significant and could not be circumvented. Moreover, it was found that the spirals also fused together into a compact bundle. The tendency of the PdCu packing to fuse together at the high temperature of this work is possibly linked to the melting point of the alloy. The 80 wt % Pd-Cu alloy has a significantly lower melting point than the pure Palladium, 1593 K and 1823 K, respectively. Consequently, the higher atomic mobility in the alloy would facilitate the fusing of the pellets.

Characterization of the PdCu pellets was performed by XRD and SEM-EDS. One of the cylindrical pellets was separated from the large agglomerate and pressed into a flat sheet for analysis by XRD. The x-ray pattern suggests that both the bulk and surface of the pellet have the same composition, i.e. 80 wt % Pd - 20 wt % Cu. A similar conclusion was reached when comparing the bulk and surface composition by SEM-EDS. However, the SEM analysis revealed an increase in the surface area (

Figure 19). The fact that the surface roughening is not as severe as that observed in the Pd pellets could be explained by the lower total time on stream for the PdCu pellets. Again, the surface roughening must be considered in the application of PdCu membranes in a membrane reactor operating in a carbon-forming zone.

Although our experimental results are not suitable for a direct comparison between the WGS in the presence of Pd and PdCu due to the differences in the gas-solid interactions in the two systems (e.g., total surface area accessible to the gas stream), the larger CO conversion observed with the fresh PdCu catalyst suggests that this material performs as a better catalyst for the reaction. The addition of palladium to copper-supported catalysts has been shown to have an enhancing effect on the WGS at low temperature³⁸. The promoting effect of the PdCu pair has been also observed in the elimination of CO and NO on ceria-zirconia-alumina-based catalysts³⁹. Such an effect was partly explained by the formation of a PdCu alloy with low Cu content. Previous theoretical work had suggested a change in the electronic configuration of Pd due to interaction with Cu⁴⁰. Additionally, studies of the WGS on single-crystal Cu surfaces have suggested that the high-temperature reaction would follow a surface-redox mechanism described by dissociative adsorption of H₂O that would provide the O species that further react with CO^{41, 42}. The dissociation of H₂O, the rate-limiting-step, is favored in less densely packed surface configurations, e.g. Cu(100) vs Cu(111)^{41, 43}. Therefore, it is tempting to speculate that the superior performance of the PdCu alloy is due to the role of the low-copper surface in the initiation of the reaction.

CONCLUSIONS

The rate of reaction of the homogeneous gas-phase forward water-gas shift reaction was studied at high-temperature (1070 – 1134 K) and both low (0.1 MPa) and

high-pressure (1.6 MPa) conditions. The rate expression was characterized by the exponents 0.5 and 1.0 for CO and H₂O, respectively. This rate expression is consistent with the proposed gas-phase mechanism of the reaction. Further, the effect of the high-pressure conditions on the reaction rate was negligible. However, our pre-exponential factor, 4.70E11 (cm³/mol)^{0.5}s⁻¹, and energy of activation, 288.3 kJ/mol, predict rate constant values that are larger than those evaluated from the gas-phase mechanism and lower than those determined from the only available gas-phase, low-pressure correlation of Graven and Long⁴. Formation of carbon inside the reactor leading to a steady increase in the reaction rate was observed. However, the carbon deposits were minimized by flowing O₂ at high-temperature between the kinetic experiments. Therefore, our slightly larger rate constants cannot be attributed to this effect. However, small deposits of carbon in the preheating section could not be removed with the oxygen treatment. Further, characterization of these deposits revealed the presence of trace amounts of nickel dispersed in the carbon. The carbon was probably formed by the Boudouard reaction whereas the nickel was extracted from the stainless steel inlet tubing via the formation and decomposition of nickel carbonyl. The presence of the small amounts of nickel would account both for the absence of a kinetic induction period and the larger rate constant values.

Confirming our previous observations on the kinetics of the reverse WGSR, Inconel[®]600 surfaces greatly enhance the reaction rate. Equilibrium conversions were attained at low-pressure conditions and temperatures as low as 973 K for residence times lower than 1 s. Therefore, the use of the gas-phase kinetic correlation would lead to significant over-estimation of the reactor volume due to this reaction rate enhancement. Surface characterization of the reactor walls indicated the formation of a chromium oxide layer in the reaction zone. In addition, nickel extraction from the preheating section through metal dusting was observed, and production of methane was found to occur in the Inconel[®]600 reactor. A preliminary correlation of the CO conversion data at temperatures in the 600 – 900 K range was achieved by assuming that the surface-catalyzed fWGSR was first order in ([CO]-[CO]_{eq}) and zero-th order in [H₂O], yielding an activation energy and a pre-exponential constant of 102.4 kJ/mol and 4.26E6 cm²/s, respectively.

The gas-phase reaction was enhanced by the presence of palladium or palladium-copper packing. However, the catalytic effect was moderate when compared to Inconel[®]600, i.e. equilibrium conversions were not achieved when the reaction was conducted in the presence of Pd or PdCu pellets with geometric surface area equal to the Inconel[®]600 reactor. The cycling between oxidizing and reducing environments significantly increased the conversions attained with the two materials. A likely explanation for the large conversions is the change in surface morphology (for Pd and PdCu) and/or the creation of porous structures inside the packing (for PdCu). Fresh PdCu appears to be a better catalyst than fresh Pd as indicated by the initial rates of reaction observed for each material.

Acknowledgements and Disclaimer

We would like to acknowledge the operational and maintenance contributions of the Parsons engineering technicians, including Ronald Hirsch, Jeremy Brannen, Ray Rokicki, Russ Miller, Brian Neel, Michael Ditillo, and Bruce Blednick. This work was sponsored through the “Transportation Fuels and Chemicals”, “Syngas Membrane Technologies,” “Gasification Technologies”, and “Hydrogen, Fuel Cells, and Infrastructure” programs within the U.S. Department of Energy. F.B. wishes to acknowledge Universidad de Antioquia for granting a leave of absence to pursue his doctoral degree.

Reference in this paper to any specific commercial product, process, or service is to facilitate understanding and does not necessarily imply its endorsement or favoring by the U.S. Department of Energy.

Literature Cited

1. Enick RM, Hill J, Cugini AV, Rothenberger KS, McIlvried HG, A model of a high temperature, high pressure water-gas shift tubular membrane reactor. ACS Preprints – Fuel Chemistry Division. 1999;44(4):919-34.
2. Enick RM, Morreale BD, Hill J, Rothenberger KS, Cugini AV, Siriwardane RV, Poston JA, Balachandran U, Lee TH, Dorris SE, Graham WJ, Howard BH, Evaluation and modeling of a high-temperature, high-pressure, hydrogen separation membrane for enhanced hydrogen production from the water-gas shift reaction,” in: Padró CEG, Lau F, Advances in hydrogen. New York, Kluwer Academic/Plenum Publishers, 2000:93-100.
3. Bustamante, F, Enick RM, Cugini AV, Killmeyer R, Howard BH, Rothenberger KS, Ciocco M, Morreale BD, Chattopadhyay S, Shi S. High temperature kinetics of the homogeneous reverse water-gas shift reaction. AIChE J. 2004;50(5):1028-41.
4. Graven, WM, Long FJ. Kinetics and mechanisms of the two opposing reactions of the equilibrium $\text{CO} + \text{H}_2\text{O} \leftrightarrow \text{CO}_2 + \text{H}_2$. J. Amer. Chem. Soc. 1954;76:2602-7. Graven, WM. Errata. J. Amer. Chem. Soc. 1954;76,6421.
5. Tingey GL. Kinetics of the water-gas equilibrium reaction. I. The reaction of carbon dioxide with hydrogen. J. Phys. Chem. 1966;70(5):1406-12.
6. Kochubei VF, Moin FB. Kinetics of the reaction of CO_2 with hydrogen. Kinetika i Kataliz. 1969;10:1203.
7. Holgate R, Tester J. Oxidation of hydrogen and carbon monoxide in sub- and supercritical water: reaction kinetics, pathways, and water-density effects. 2. Elementary reaction modeling. J. Phys. Chem. 1994;98:810-22.
8. Newsome D. The water-gas shift reaction. Catal. Rev. Sci. Eng. 1980;21(2):275-381.
9. Xu J, Froment GF. Methane steam reforming, methanation and water-gas shift: I. Intrinsic kinetics. AIChE J. 1989;35(1):88-96.
10. Salmi T, Hakkarainen R. Kinetic study of the low-temperature water-gas shift reaction over a Cu-ZnO catalyst. Appl. Catal. 1989;49(2):285-306.
11. Keiski RL, Desponds O, Chang YF, Somorjai GA. Kinetics of the water-gas shift reaction over several alkane activation and water-gas shift catalysts. Appl.

- Catal. A. 1993;101(2):317-38.
12. Rhodes C, Hutchings GJ, Ward AM. Water-gas shift reaction: finding the mechanistic boundary. *Catal. Today*. 1995;23:43-48.
 13. Lund CRF. The microkinetics of water-gas shift over sulfided Mo/Al₂O₃ catalysts. *Ind. Eng. Chem. Res.* 1996;35(8):2531-8.
 14. Bunluesin T, Gorte RJ, Graham GW. Studies of the water-gas-shift reaction on ceria-supported Pt, Pd, and Rh: implications for oxygen-storage properties. *Appl. Catal. B.* 1998;15(1-2):107-14.
 15. Li Y, Fu Q, Flytzani-Stephanopoulos M. Low-temperature water-gas shift reaction over Cu- and Ni-loaded cerium oxide catalysts. *Appl. Catal. B.* 2000;27(3):179-91.
 16. Hadman G, Thompson HW, Hinshelwood CN. The oxidation of carbon monoxide. *Proc. Roy. Soc. (London)* 1932;A137:87-101.
 17. Bradford BW. The water-gas reaction in low-pressure explosions. *J. Chem. Soc.*, 1933:1557.
 18. Long FJ, Sykes KW. The catalysis of the carbon monoxide-steam reaction. *Proc. Roy. Soc. (London)* 1952;A215:111-9.
 19. GRI-Mech 3.0. http://www.me.berkeley.edu/gri_mech/ 2000.
 20. Ingles OG. The water gas shift reaction in fuel systems. Part 1. The water gas shift reaction on carbon. *Trans. Faraday Soc.* 1952;48:706.
 21. Kondratjev V, Ziskin M. On the reaction of water gas conversion in quartz vessels. *Acta Physicochim.* 1943;18:197.
 22. Long FJ, Sykes KW. The mechanism of the steam-carbon reaction. *Proc. Roy. Soc. (London)* 1948;A193:377-99.
 23. Zhu ZH, Finnerty J, Lu GQ, Wilson MA, Yang RT. Molecular orbital theory calculations of the H₂O-carbon reaction. *Energy & Fuels*, 2002;16:847-54.
 24. Ridler DE, Twigg MV. Steam reforming. In: Twigg MV. *Catalyst Handbook*, (2nd edition). London: Manson Publishing, 1996:225-80.
 25. Miksa D, Brill T. Spectroscopy of hydrothermal reactions 17. kinetics of the surface-catalyzed water-gas shift reaction with inadvertent formation of Ni(CO)₄. *Ind. Eng. Chem. Res.* 2001;40:3098-103.
 26. Sykes ML, Edwards IAS, Thomas KM. Metal carbonyl decomposition and carbon deposition in the advanced gas-cooled nuclear reactor. *Carbon*. 1993;31(3):467-72.
 27. King PJ, Doyle DM. High temperature gaseous oxidation for passivation of austenitic alloys. US Patent 6,488,783. 2002.
 28. Fogler HS. *Elements of chemical reaction engineering*, second edition. Upper Saddle River, NJ: Prentice Hall PTR. 1992:573-578.
 29. Voogt EH, Mens AJM, Gijzeman OLJ, Geus JW. Adsorption of oxygen and surface oxide formation on Pd(111) and Pd foil studied with ellipsometry, LEED, AES and XPS. *Surf. Sci.* 1997;373:210-20.
 30. Vesper G, Wright A, Caretta R. On the oxidation-reduction kinetics of palladium. *Catal. Lett.* 1999;58:199-206.
 31. Wolf MM, Zhu H, Green WH, Jackson GS. Kinetic model of polycrystalline Pd/PdO_x in oxidation/reduction cycles. *Appl. Catal. A.* 2003;244:323-40.
 32. Peuckert M. Study on surface and bulk palladium oxide, its thermal stability, and

- a comparison with other noble metal oxides. *J. Phys. Chem.* 1985;89:2481-6.
33. Aggarwal S, Monga AP, Perusse SR, Ramesh R, Ballarotto V, Williams ED, Chalamala BR, Wei Y, Reuss RH. Spontaneous ordering of oxide nanostructures. *Science* 2000;287:2235-7.
 34. Monteiro RS, Zemylanov D, Storey JS, Ribeiro FH. Surface area increase on Pd foils after oxidation in excess methane. *J. Catal.* 2001;201:37-45.
 35. Matolin V, Rebholz M, Kruse N. Defect-induced dissociation of CO on palladium. *Surf. Sci.* 1991;245:233-43.
 36. Morreale BD, Ciocco MV, Howard BH, Killmeyer RP, Cugini AV, Enick RM. Effect of hydrogen-sulfide on the hydrogen permeance of palladium-copper alloys at elevated temperatures. *J. Membr. Sci.* 2004;241/2:219-24.
 37. Howard BH, Killmeyer RP, Cugini AV, Morreale BD, Ciocco MV, Enick RM. Hydrogen permeance of palladium-copper alloy membranes over a wide range of temperatures and pressures. *J. Membr. Sci.* 2004;241/2:207-18.
 38. Bickford ES, Velu S, Song C. Ceria-supported Cu-Pd bimetallic catalysts for oxygen-assisted water-gas-shift reaction for proton-exchange membrane fuel cells. *ACS Preprints – Fuel Chemistry Division.* 2003;48(2):810-1.
 39. Hungria AB, Iglesias-Juez A, Martinez-Arias A, Fernandez-Garcia M, Anderson JA, Conesa JC, Soria J. Effects of copper on the catalytic properties of bimetallic Pd-Cu(Ce,Zr)Ox/Al₂O₃ and Pd-Cu(Ce,Zr)Ox catalysts for CO and NO elimination. *J. Catal.* 2002;206:281-94.
 40. Fernandez-Garcia M, Conesa JC, Clotet A, Ricart JM, Lopez N, Illas F. Study of the heterometallic bond nature in PdCu(111) surfaces. *J. Phys. Chem. B.* 1998;102,141-7.
 41. Jakdetchai O, Nakajima T. Mechanism of the water-gas shift reaction over Cu(110), Cu(111) and Cu(100) surfaces: an AM1-d study. *J. Molec. Struct. (Theochem).* 2002;619:51-8.
 42. Fishtik I, Datta R. A UBI-QEP microkinetic model for the water-gas shift reaction on Cu(111). *Surface Science.* 2002;512:229-54.
 43. Wang G, Jiang L, Cai Z, Pan Y, Zhao X, Huang W, Xie K, Li Y, Sun Y, Zhong B. Surface structure sensitivity of the water-gas shift reaction on Cu(hkl) surfaces: a theoretical study. *J. Phys. Chem. B.* 2003;107:557-62.

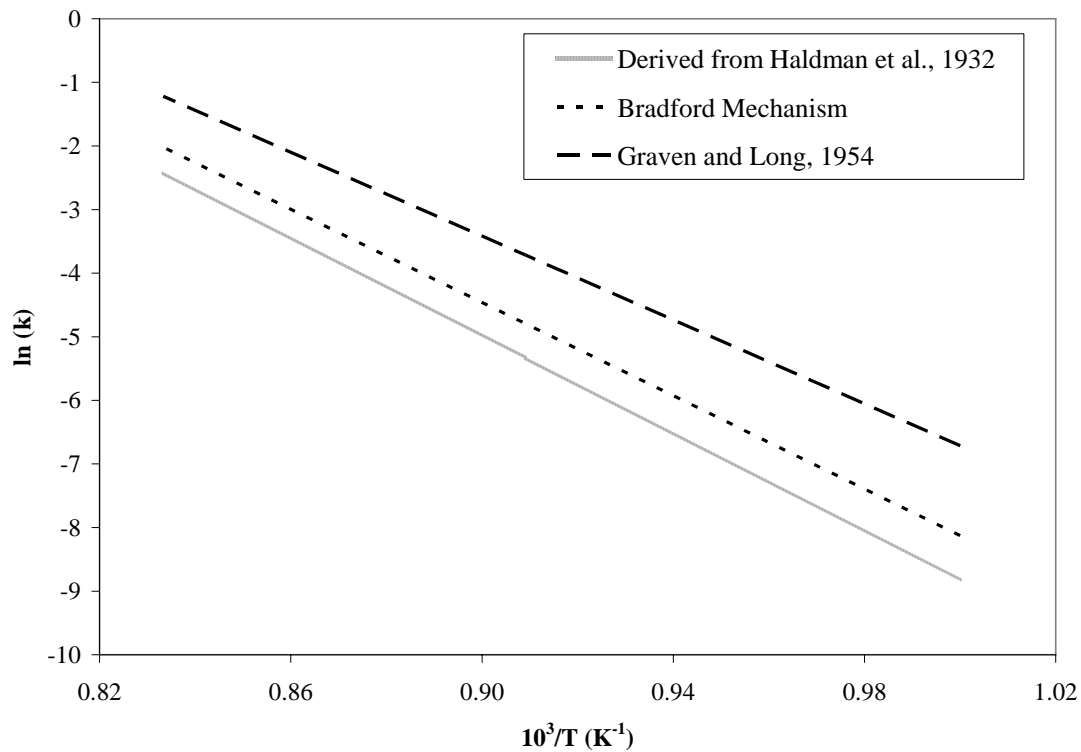


Figure 1. Arrhenius representations of the fWGSR rate constant presented in a literature correlation (Graven and Long⁴), extracted from literature data (Haldman¹⁶) and based on the Bradford¹⁷ mechanism combined with GRI database¹⁹ values for individual rate constants, Equation 6. Units of k are $[(\text{L/mol})^{0.5} \text{ s}^{-1}]$.

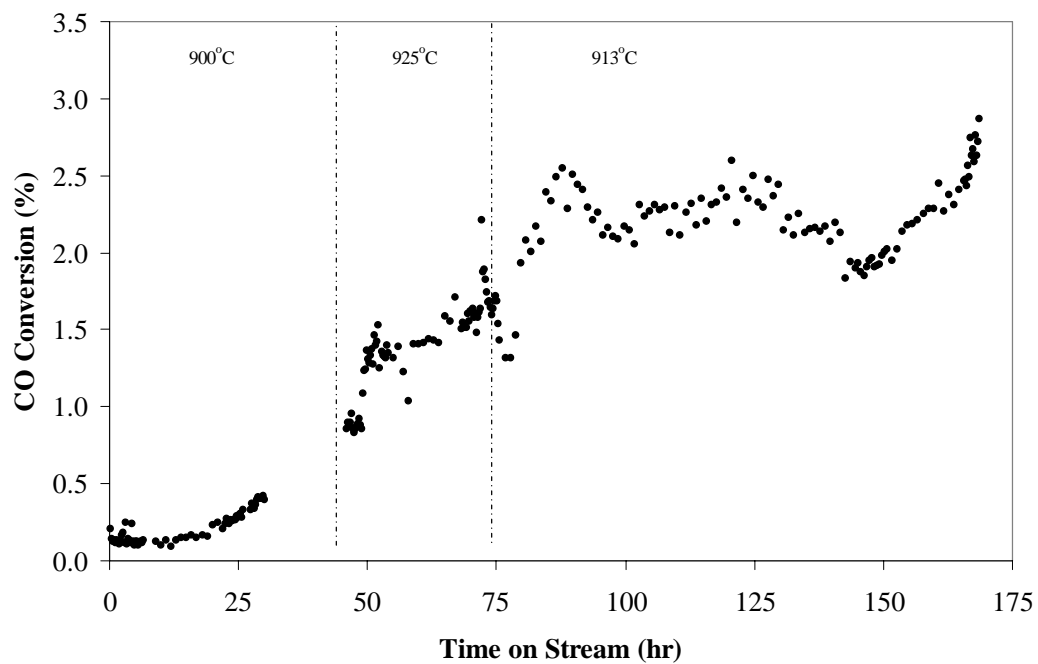


Figure 4. Increase of reaction rate with time on stream, fWGSR in a quartz reactor. Pressure, 0.101 MPa. Residence time, 0.22 s. Inlet composition, $y_{\text{CO}} = 0.85$, $y_{\text{H}_2\text{O}} = 0.15$, $y_{\text{CO}_2} = y_{\text{H}_2} = 0$. Only data collected during early times ($t < 8$ hours) were used in kinetic study because they were considered to be unaffected by the accumulation of carbon.

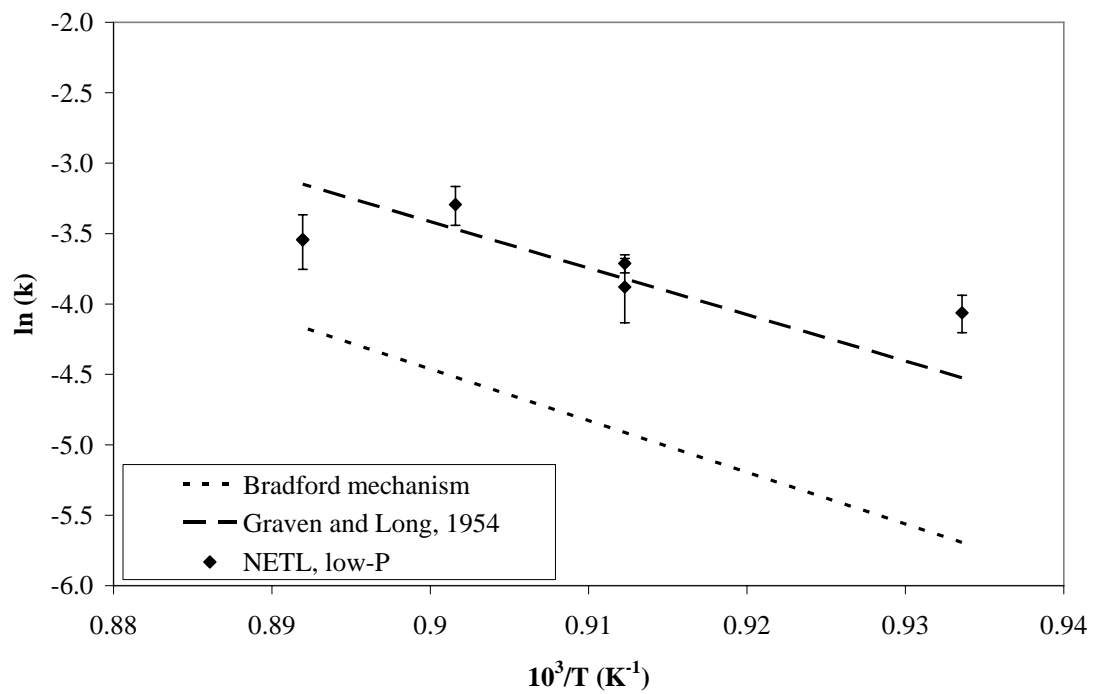


Figure 5. Comparison of NETL low pressure fWGSR (0.1 MPa) results with results of Graven and Long⁴ and with results obtained using Equation 7, which is based on the Bradford¹⁷ mechanism and individual reaction rate constants from the GRI database¹⁹. Units of k are $[(\text{L/mol})^{0.5} \text{ s}^{-1}]$.

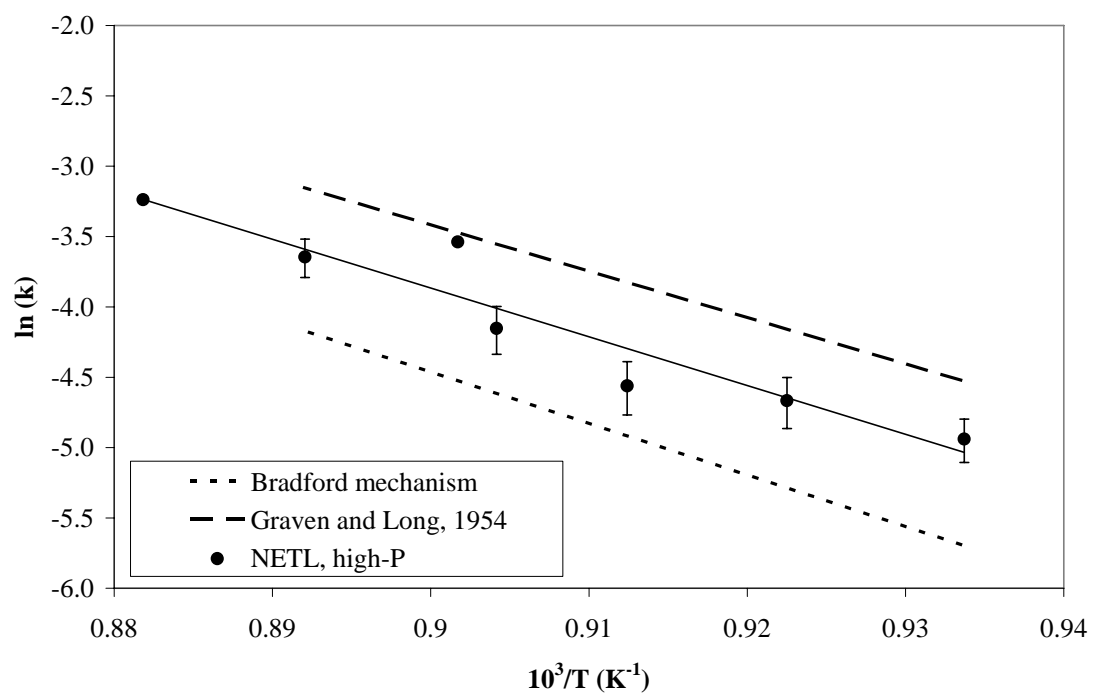


Figure 6. Rate constant of the high-temperature, high-pressure (1.6 MPa) fWGSR in an empty quartz reactor and a quartz-packed quartz reactor as a function of inverse absolute pressure. Results from the experimental correlation by Graven and Long⁴ and calculated from the gas-phase mechanism by using the GRI¹⁹ values are given as comparison. Units of k are $[(\text{L/mol})^{0.5} \text{s}^{-1}]$.

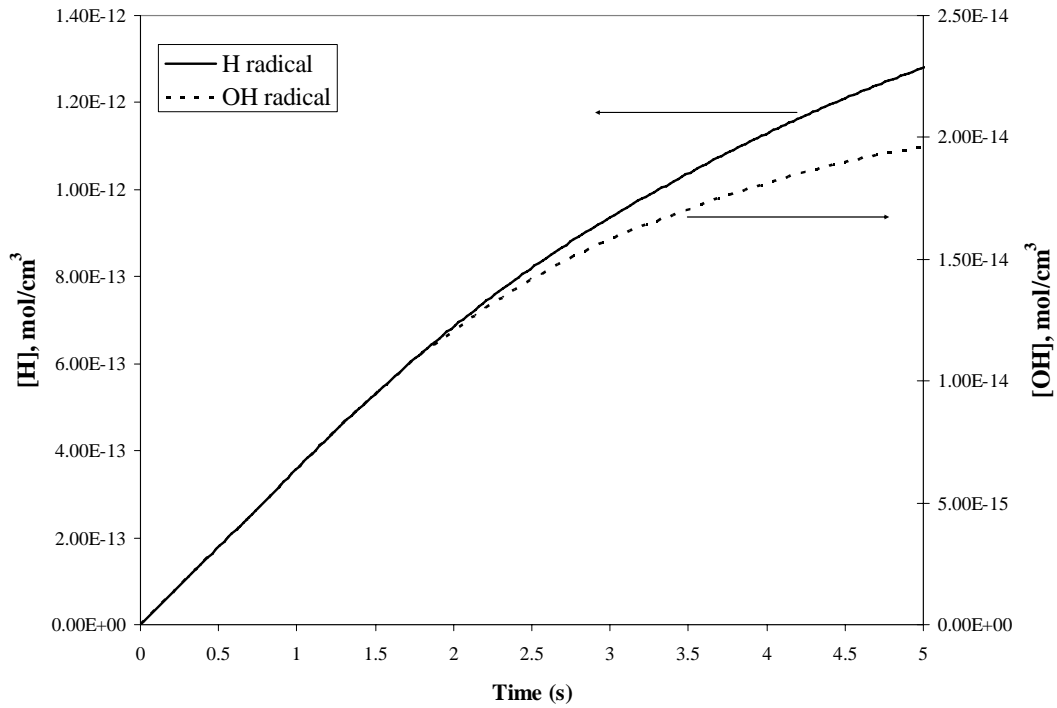


Figure 7. Concentration profiles for H and OH species as a function of reaction time as obtained by numerical solution of the Bradford mechanism. Temperature (1173 K), pressure (1.6 MPa), and inlet molar fractions ($y_{\text{CO}} = 0.77$, $y_{\text{H}_2\text{O}} = 0.23$, $y_{\text{CO}_2} = y_{\text{H}_2} = 0$) similar to the experiments.

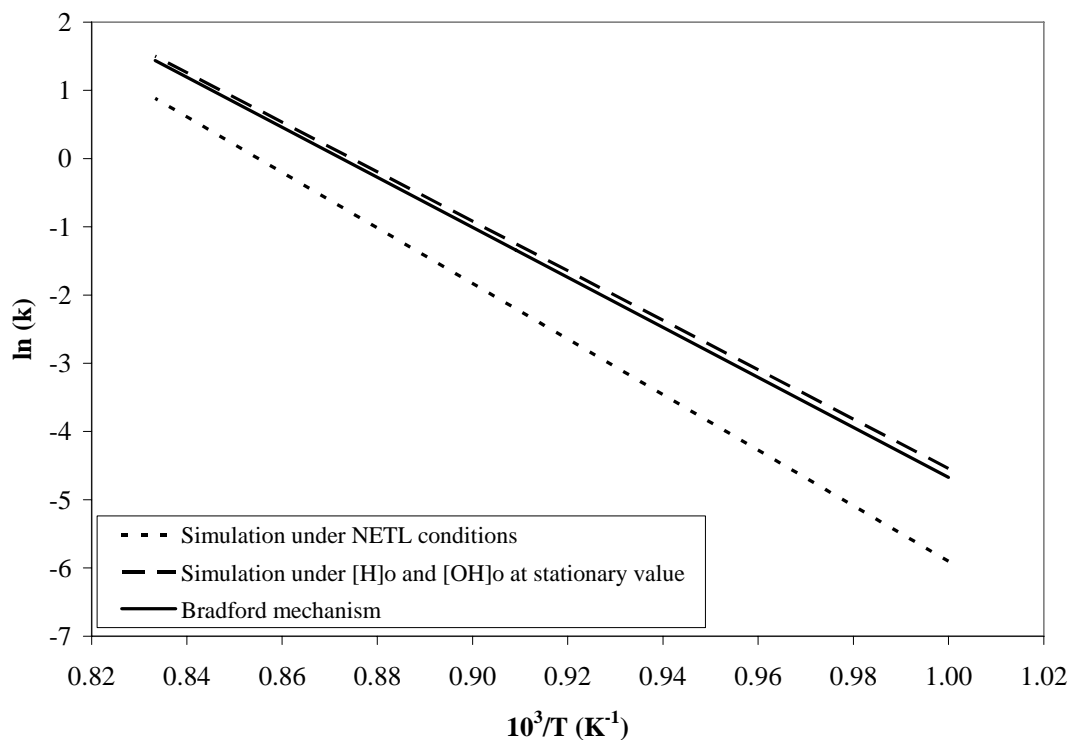


Figure 8. Rate constant of the high-temperature, high-pressure (1.6 MPa) fWGSR in a quartz reactor as a function of inverse absolute temperature. Results of the simulation of the gas-phase mechanism with and without forcing stationary-state values for the concentration of H and OH at the inlet of the reactor. Values evaluated from the gas-phase mechanism are given by comparison. Units of k are $[(\text{cm}^3/\text{mol})^{0.5} \text{ s}^{-1}]$.

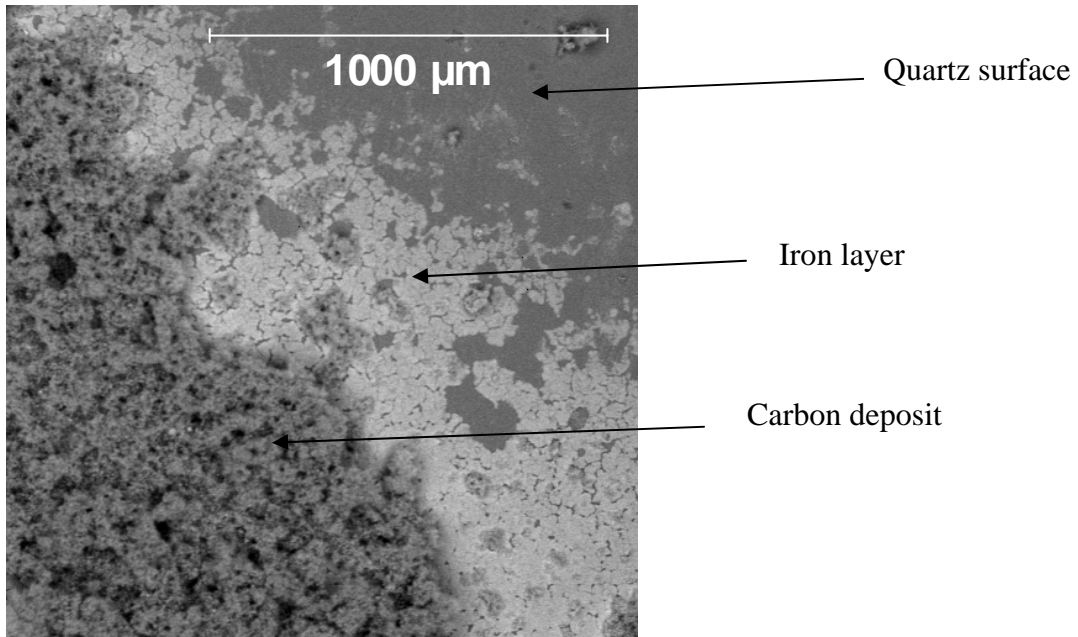


Figure 9. SEM-EDS characterization of the carbon deposit on the preheating section.

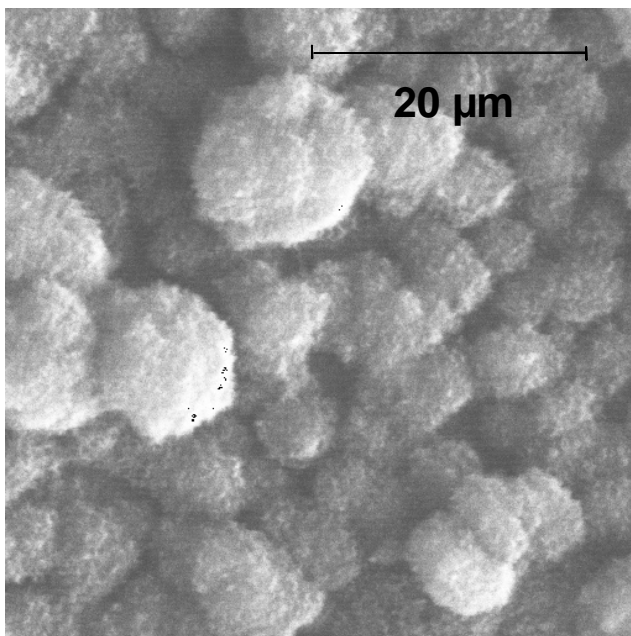


Figure 10. SEM image of the carbon particles deposited at the inlet of the reactor.

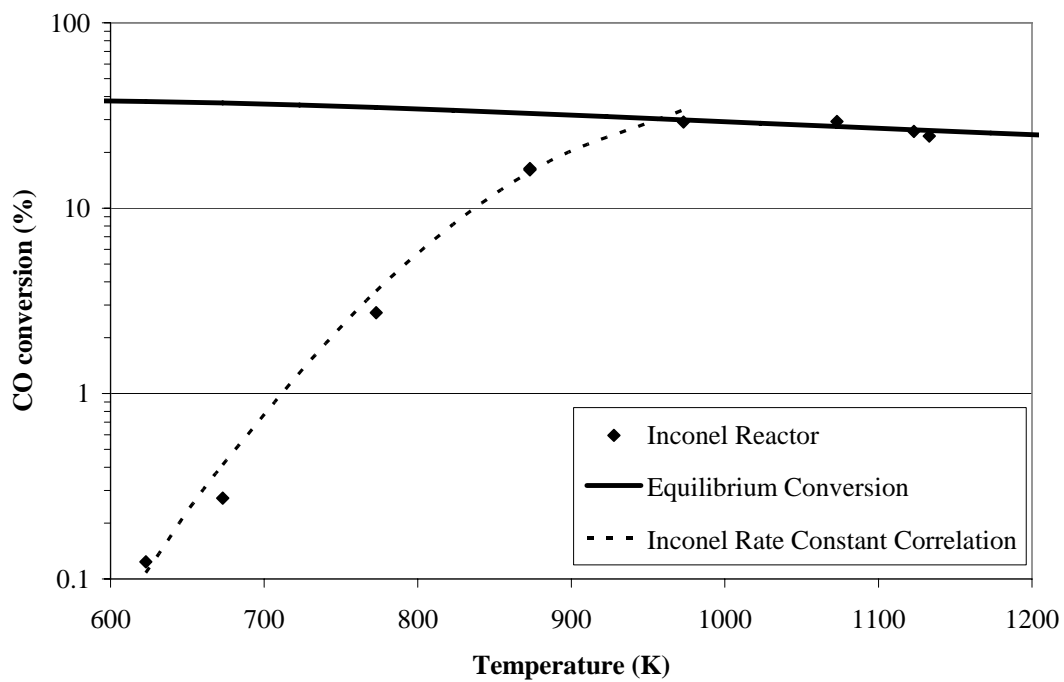


Figure 11. Low-pressure (0.1 MPa) fWGSR in an Inconel[®] 600 reactor. Inlet composition, $y_{\text{CO}} = 0.77$, $y_{\text{H}_2\text{O}} = 0.23$, $y_{\text{CO}_2} = y_{\text{H}_2} = 0$. Residence time < 1s.

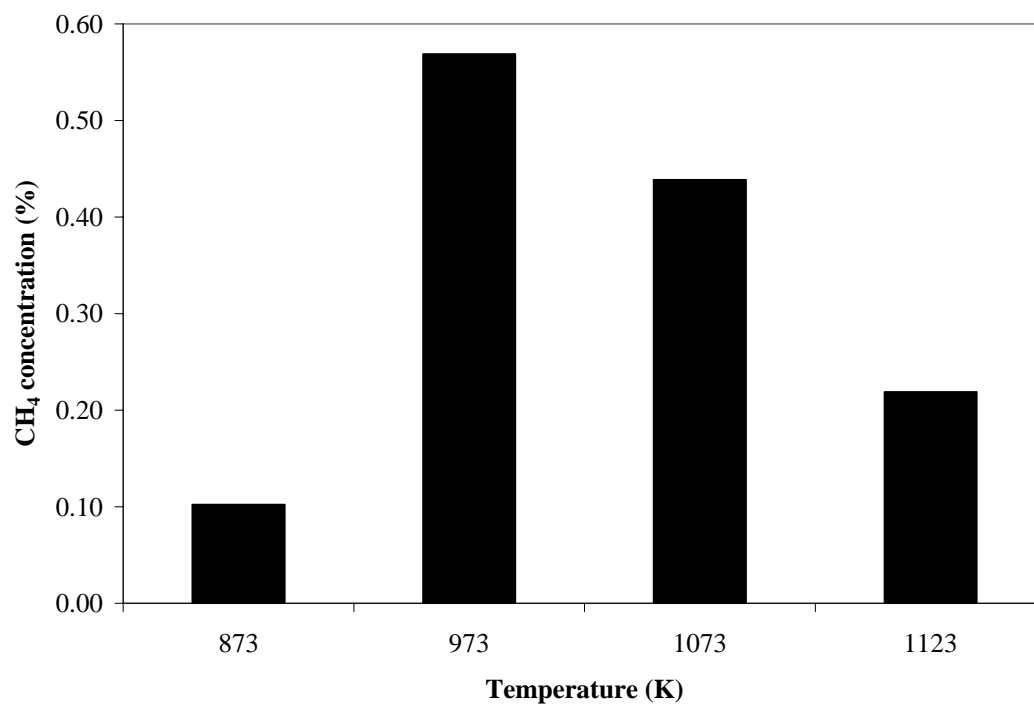


Figure 12. Formation of methane via side reaction(s) in the low-pressure water-gas shift reaction carried out in an Inconel[®] 600 reactor; effluent CH₄ composition as a function of reaction temperature. Conditions are similar to those in Figure 11.

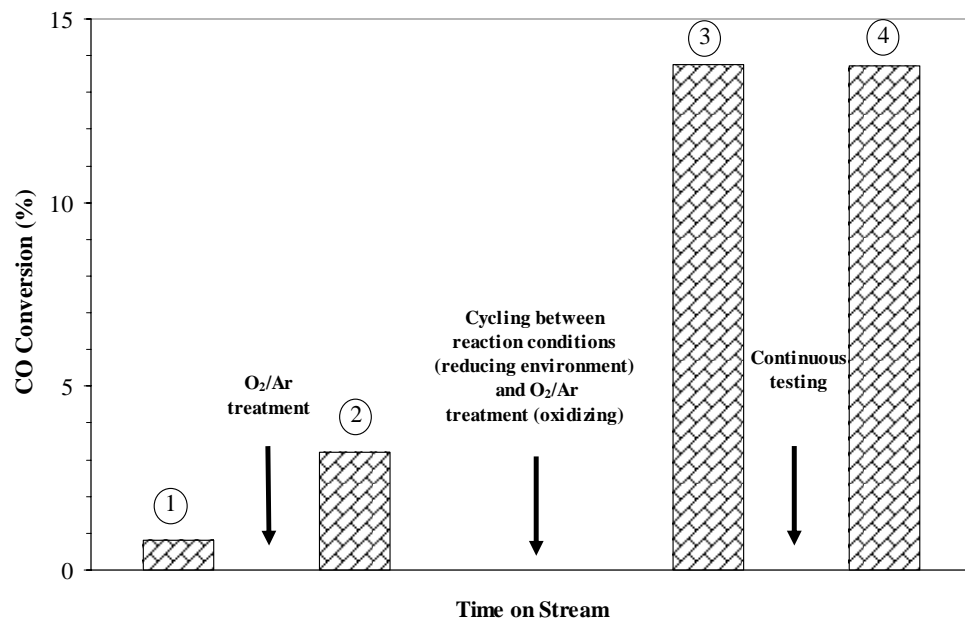


Figure 13. CO conversions for the WGSR in a Pd-packed, quartz reactor. Temperature, 1173 K; ambient pressure; residence time, 0.25 s. Inlet composition, $y_{\text{CO}} = 0.77$, $y_{\text{H}_2\text{O}} = 0.23$, $y_{\text{CO}_2} = y_{\text{H}_2} = 0$. Gas-phase conversions are below 0.3%. CO equilibrium conversion is 35%.

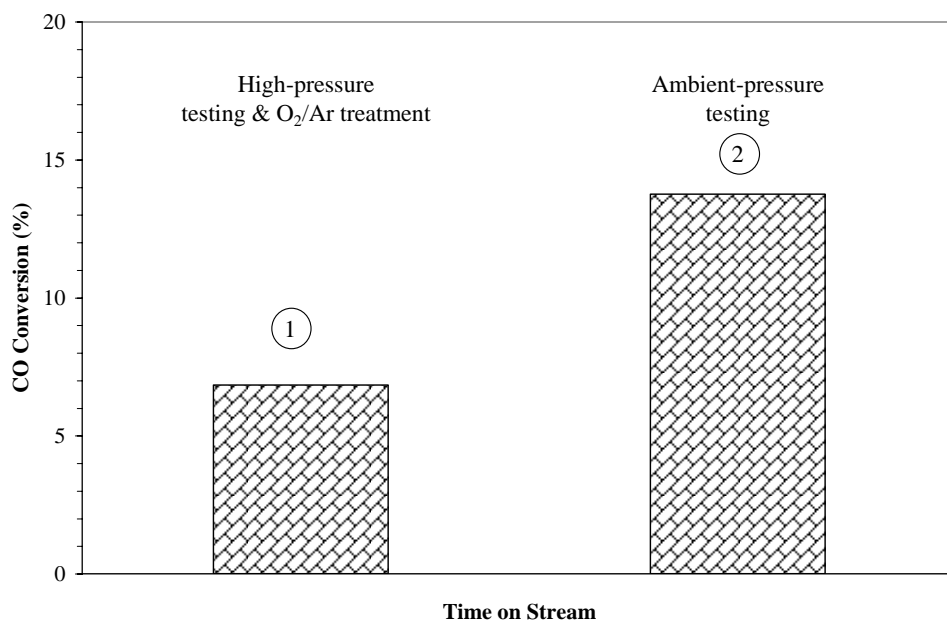


Figure 14. Effect of the duration of the O₂/Ar treatment on the conversions observed in the Pd-packed reactor. Packing was treated in the oxidizing environment for 66 hr between the two data sets. Temperature, 1123 K. Residence time: 0.22 s (low-pressure), 1.7 s (high-pressure). Inlet composition, $y_{\text{CO}} = 0.77$, $y_{\text{H}_2\text{O}} = 0.23$, $y_{\text{CO}_2} = y_{\text{H}_2} = 0$. Gas-phase conversions are below 0.75%. CO equilibrium conversion is 21% for data set 1 and 29% for data set 2.

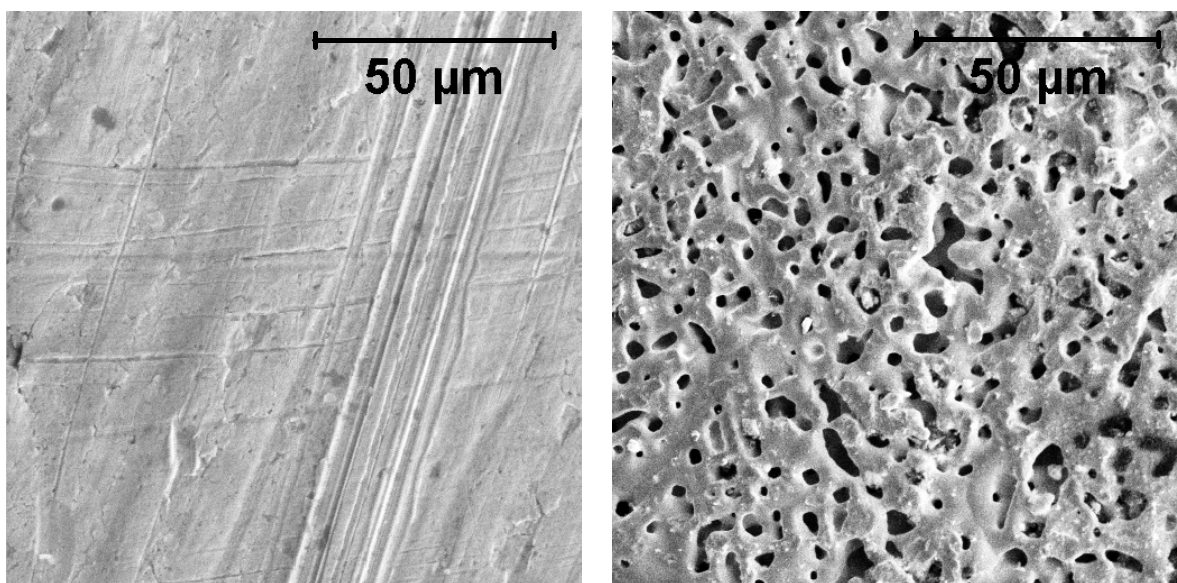


Figure 15. SEM images of the fresh (left) and used (i.e., after reaction studies) Pd packing (right).

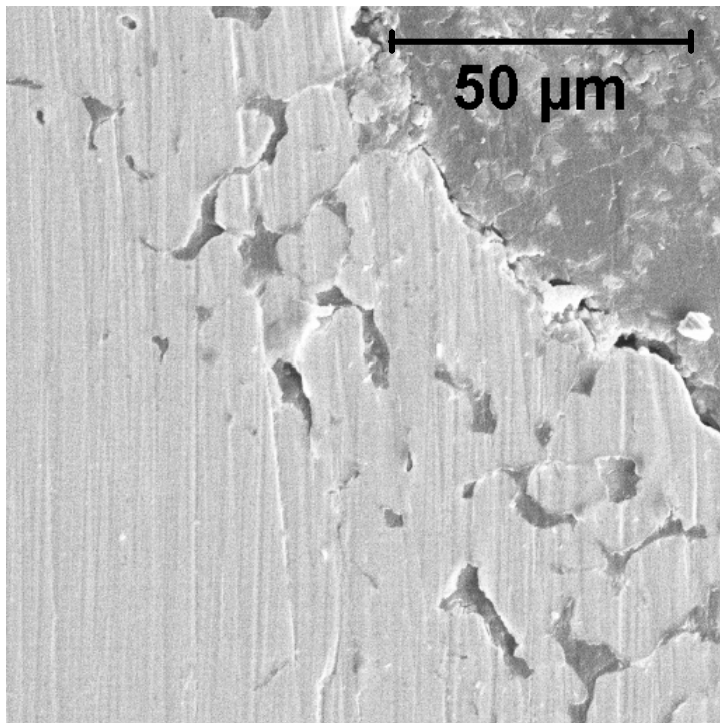


Figure 16. SEM cross-sectional view of the Pd-packing after reaction. The packing was encased in a polymer resin and polished.

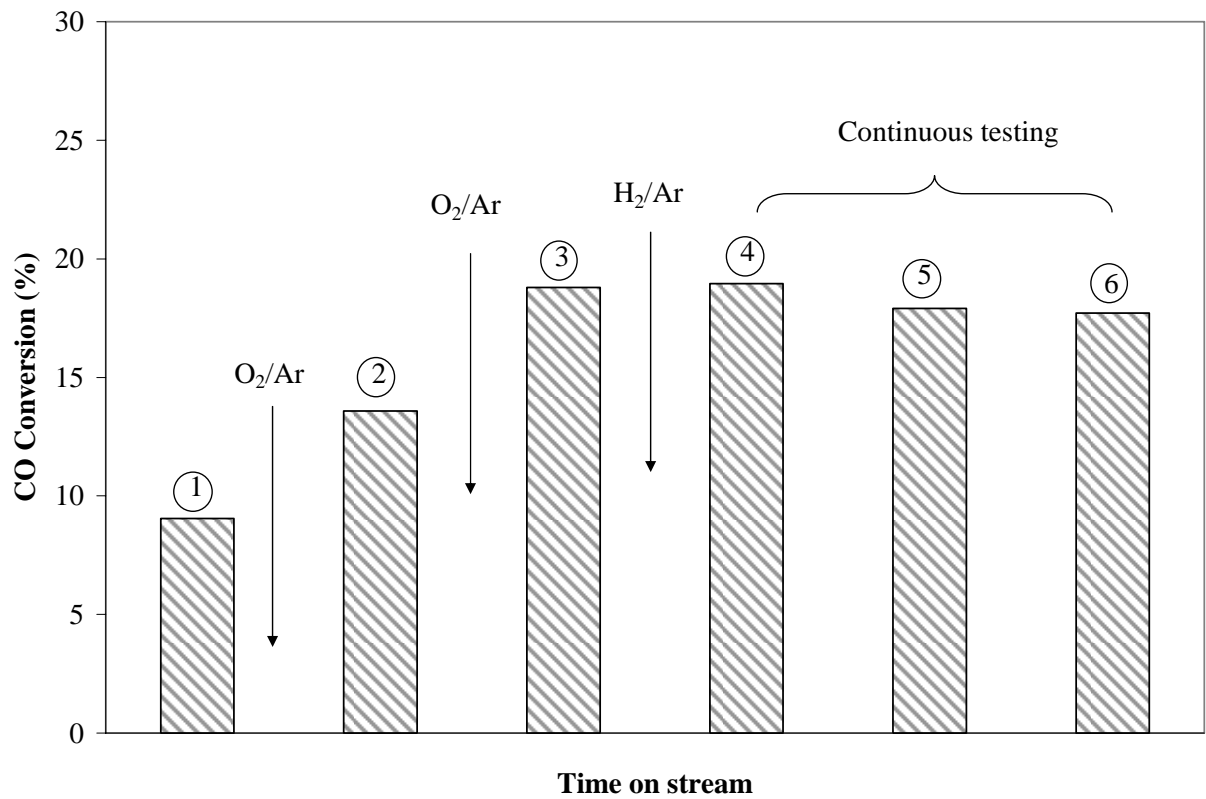


Figure 17. WGSR in the presence of PdCu packing. Temperature, 1173 K; ambient pressure; residence time, 0.25 s. Inlet composition, $y_{\text{CO}} = 0.77$, $y_{\text{H}_2\text{O}} = 0.23$, $y_{\text{CO}_2} = y_{\text{H}_2} = 0$. Gas-phase conversions are below 0.3%. CO equilibrium conversion is 35%.

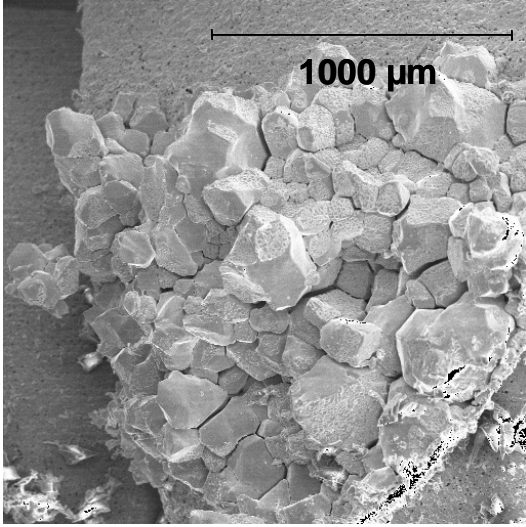


Figure 18. SEM image of the internal structure of a fractured PdCu pellet.

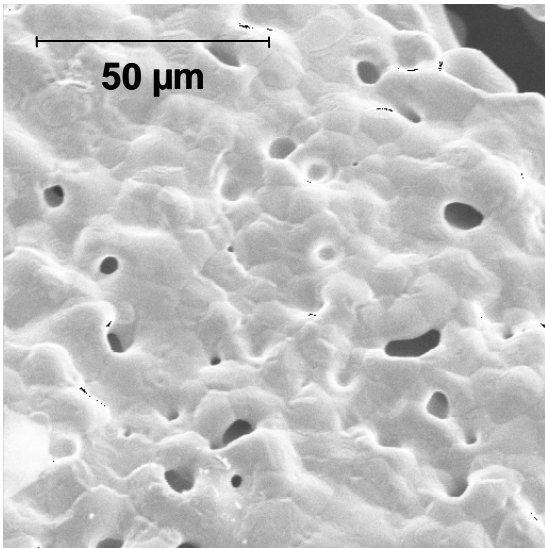


Figure 19. SEM image of the surface of a PdCu pellet after reaction.

Table 1. Pre-exponential constant and activation energy of the fWGSR rate constant – gas-phase mechanism and experimental results. Pre-exponential factor, $(\text{cm}^3/\text{mol})^{0.5} \text{ s}^{-1}$; Energy of Activation, kJ/mol, kcal/mol.

Reference	Temperature K	Pressure MPa	Pre- exponential Factor $(\text{cm}^3/\text{mol})^{0.5} \text{ s}^{-1}$	Energy of Activation kJ/mol
Hadman et al., 1932*	973 – 1073	0.101	2.22E14	319.2
Graven and Long, 1954	1073 – 1373	0.101	7.97E12	274.1
Bradford mechanism and GRI rate constants, Eq. 6			7.68E13	304.6
This work (experimental results)	1070-1134	1.6	7.40E11	288.3

* Rate constant was evaluated from the reaction time and conversion data reported in the reference, using the Bradford exponents for CO and H₂O.